Electrochimica Acta 182 (2015) 652–658

Contents lists available at ScienceDirect

Electrochimica Acta

journal homepage: www.elsevier.com/locate/electacta

Three-dimensional MoS_2/rGO hydrogel with extremely high double-layer capacitance as active catalyst for hydrogen evolution reaction

Junma Zhang[a], Li Zhao[a], Aiping Liu[a,b,*], Xiaoyun Li[a], Huaping Wu[c], Congda Lu[c]

[a] Center for Optoelectronics Materials and Devices, Zhejiang Sci-Tech University, Hangzhou 310018, China
[b] State Key Lab of Silicon Materials, Zhejiang University, Hangzhou 310027, China
[c] Key Laboratory of E&M (Zhejiang University of Technology), Ministry of Education & Zhejiang Province, Hangzhou 310014, China

ARTICLE INFO

Article history:
Received 13 May 2015
Received in revised form 26 September 2015
Accepted 26 September 2015
Available online 30 September 2015

Keywords:
Three-dimensional hydrogel
MoS_2/rGO hybrids
hydrogen evolution reaction
hydrothermal method

ABSTRACT

Three-dimensional (3D) molybdenum disulfide/reduced graphene oxide (MoS_2/rGO) hydrogels were developed by a simple and controllable one-pot hydrothermal method. The MoS_2 nanosheets were uniformly anchored on the 3D rGO framework with strong adhesion. The obtained MoS_2/rGO hydrogel with optimized rGO percentage showed extremely high double-layer capacitance about 29.60 mF/cm^2 due to the special 3D network structure. Electrochemical measurements confirmed that the MoS_2/rGO hydrogel exhibited excellent electrocatalytic activity for hydrogen evolution reaction (HER) with a small onset overpotential of 125 mV and Tafel slope of 41 mV/decade, indicating the Volmer-Heyrovsky mechanism during the HER process and the electrochemical desorption step as rate-limiting step. Our results demonstrated that the 3D MoS_2/rGO hydrogel could not only provide rich active sites for HER due to the inhibition of re-stacking process of (0 0 2) planes of MoS_2 nanosheets along the C-axis, but also greatly contribute to the enlarged electrochemical surface area because of the formation of 3D network structure in the self-assembly process. This may open up a potential way to design advanced materials for HER.

1. Introduction

The increasing demand for clean, earth-abundant and renewable energy resources has triggered great attention due to the excessive consumption of traditional nonrenewable fossil fuels [1–3]. Hydrogen has been considered as an ideal alternative energy carrier with exceedingly high energy density [1,4]. Especially, electrocatalytic hydrogen evolution reaction (HER) is regarded as one of the most efficient technologies to generate hydrogen during water splitting [5–9]. Up to now, noble metals electrocatalysts based on platinum exhibit the zero-closed overpotential and largest current density during the HER process. However, the high cost and extraordinary scarcity greatly hinder their practical application in the near future [1,8,9]. Thus, developing an advanced and effective electrocatalyst with abundant and inexpensive raw materials to replace the rare and precious metals for boosting the energy economy still remains urgent [1,5,10]. In recent years, transition metal sulfides have attracted tremendous attention for their intriguing chemical and physical properties. Among these, molybdenum disulfide (MoS_2) is regarded as a potential HER catalyst for its relatively low adsorption free energy for proton [3]. In the past decades, some pioneering works have been carried out through both theoretical calculation [11] and experiments [12], which confirms that the catalytic active sites stem from the edges of (0 0 2) crystallographic planes of MoS_2 [1,12–14]. Hence, designing MoS_2 nanostructures with more edge sites is one effective strategy to obtain a perfect HER electrocatalyst. Numerous efforts have been made based on this purpose [5,13]. For example, Xie and her coworkers synthesized the ultrathin MoS_2 nanosheets with additional active sites by a simple solvothermal method [13], resulting in excellent HER activity compared with the ones with less active sites. However, as a p-type semiconductor, MoS_2 exhibits extremely poor conductivity [15], especially along the two adjacent basal planes, whose resistance is expected to be 10 orders of magnitude larger than that of single basal plane [3]. From such consideration, improved conductivity and limited layers seem to be a key factor to optimize the catalytic activity of MoS_2 electrocatalysts.

Graphene, a typical two-dimensional material with only one atom thickness, has a theoretically calculated surface area of

* Corresponding author. Tel.: +86 571 86843574; fax: +86 571 86843574.
E-mail address: liuaiping1979@gmail.com (A. Liu).

http://dx.doi.org/10.1016/j.electacta.2015.09.147
0013-4686/

2630 $m^2 g^{-1}$, excellent high conductivity and strong mechanical properties, which makes it suitable for loading and confining nanosized materials [16]. Recently, three-dimensional (3D) graphene, a framework of connecting graphene sheets, has attracted great interest in energy application [17] due to its ultrahigh surface-to-volume ratio, high porosity, strong mechanical strength, excellent electrical conductivity and fast mass and electron transport kinetics. 3D graphene-based composites have been successfully applied in various electrochemical energy storage devices, such as supercapacitors [18], Li-ion batteries [19] and fuel cells [20]. Recently, 3D MoS_2/graphene or MoS_2/reduced graphene oxide (MoS_2/rGO) composites have been widely synthesized through various ways, such as hydrothermal process [21,22], electrochemical deposition [23,24] and chemical vapor deposition [25]. The graphene or rGO inhibits the aggregation of MoS_2 nanosheets and favors the formation of nanostructured MoS_2 with rich active sites during the hydrothermal process, consequently leading to an increase of HER catalytic activity [5,13,14]. Since the amounts of GO and thiourea precursors greatly affect the 3D framework, electroactive area and active sites of MoS_2/rGO hydrogel [13,21], suitable controlling for the component of precursors is therefore crucial for morphology and performance modulations of hybrids. However, the study of GO (or rGO) content effect on morphology and HER catalytic performance of MoS_2/rGO composite electrocatalyst is still limited [21,22].

In this work, we demonstrate a facile strategy to fabricate 3D MoS_2/rGO hydrogel by one-pot hydrothermal method. The highly conductive network of rGO matrix and strong interaction between MoS_2 and rGO enable the as-prepared 3D MoS_2/rGO hydrogels to be both efficient and acidic stable in HER. The effect of rGO content on the structures and catalytic performance of MoS_2/rGO hydrogel for HER is carefully investigated by changing the concentration of GO in the precursors. The as-obtained MoS_2/rGO with appropriate ratio of C:Mo exhibits extremely high HER performance with a current density of 12 mA/cm^2 (45 A/g) at an overpotential of 200 mV and rather small Tafel slope as low as 41 mV/decade in contrast with other samples. Furthermore, the turnover frequency (TOF) and double-layer capacitance (C_{dl}) of MoS_2/rGO hybrids are investigated to further illustrate the synergistic effect between MoS_2 and rGO in the hydrogel.

2. Experimental

2.1. Regents

Graphite powder (256 mesh) was supplied by Qingdao Huatai Tech. Co. Ltd. Sulfuric acid (H_2SO_4 98%), sodium nitrate ($NaNO_3$), potassium permanganate ($KMnO_4$) and sodium sodium molybdate ($Na_2MoO_4.2H_2O$) were purchased from Sigma-Aldrich. Thiourea (H_2NCSNH_2) was supplied by Shandong Shuangshuang Chemical Co. Ltd. All of the reagents were of analytical grade and used without further purification.

2.2. Preparation of 3D MoS_2/rGO hydrogels

GO was prepared by the modified Hummers' method [26]. The 3D MoS_2/rGO hydrogels were synthesized by a simple hydrothermal process. Briefly, a certain amount of as-prepared GO solution (7.5 mg/ml) in the reagent bottle was mixed with 0.15 g of $Na_2MoO_4{\cdot}2H_2O$ and 0.3 g of H_2NCSNH_2. Then additional DI water was added to the mixture to keep the total volume of final suspension of 15 ml. After that, the suspension was transferred to a Teflon-lined stainless steel autoclave and maintained at 220 °C for 20 h, followed by naturally cooling down to room temperature. The obtained hydrogels were washed with DI water several times and freeze-dried overnight. The catalyzer powers were collected by centrifugation at 8000 rpm for 5 min with DI water. The washing step was repeated for five times to remove any possible unreacted ions. Changing the volumes of GO solution in the reaction system from 1 ml to 4 ml, the MoS_2/rGO hybrids with different MoS_2/rGO mass ratios were obtained and labeled as MoS_2/rGO_x (x = 1–4), respectively. The pristine MoS_2 as comparison was prepared in a similar procedure.

2.3. Structural and performance characterization of 3D MoS_2/rGO hydrogels

The morphologies and components of different MoS_2/rGO composites were observed by a Field emission scanning electron microscope (FESEM, Hitachi S4800) equipped with an energy-dispersive X-ray spectroscopy (EDS). Transmission electron

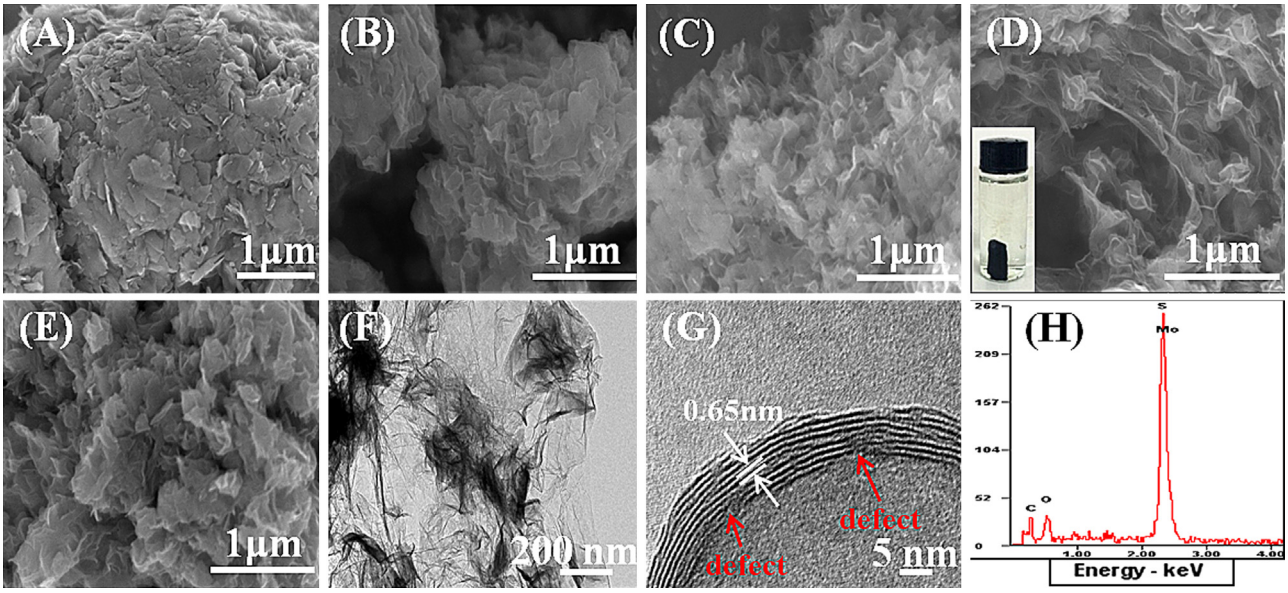

Fig. 1. Scanning electron microscopy images of (A) MoS_2, (B) MoS_2/rGO_1, (C) MoS_2/rGO_2, (D) MoS_2/rGO_3 and (E) MoS_2/rGO_4. The inset in (D) is the digital photograph of 3D MoS_2/rGO_3 hydrogel. (F) TEM and (G) corresponding HRTEM images of as-prepared MoS_2/rGO_3. (H) Energy dispersive spectrum of 3D MoS_2/rGO_3 hydrogel.

microscopy (TEM) images were collected on a Hitachi H-7650 at an acceleration voltage of 200 kV. X-ray diffraction (XRD) measurements were performed on a X-ray diffractometer (Bruker AXS D8) using the Cu Ka radiation (λ = 0.15418 nm), with the 2θ scan from 10° to 80° at a step of 0.02°. Fourier transform infrared (FTIR) spectroscopy was obtained on a Nicolet Avatar 370 spectrometer. Raman spectra were recorded on a Thermo Fisher DXR Raman spectrometer equipped with an objective (50×) using a He-Ne laser (λ = 632.8 nm). X-ray photoelectron spectroscopy (XPS) was collected by a KRATOS AXIS ULTRA-DLD with the binding energy calibrated by C1s as reference energy (C1s = 284.6 eV).

For electrode preparation, 4 mg of the catalyst power and 80 μl Nafion solution (5 wt.%) were dispersed in 1 ml water-ethanol solution with volume ratio of 3:1 and sonicated for 1 h to form a homogeneous catalyst ink. Then 5 μl of the black ink (containing 20 μg of catalyst) was drop-casted onto a glassy carbon electrode (GCE) with 3 mm in diameter (loading ca. 0.284 mg cm^{-2}). All electrochemical measurements were conducted on a CHI 660D electrochemical work station (Shanghai Chenhua Instrument Co., China) in a standard three-electrode setup at room temperature. The catalyst anchored GCE was used as the working electrode. A saturated calomel electrode (SCE) and a Pt wire were used as the reference electrode and counter electrode, respectively. Linear sweep voltammetry measurement was conducted in a 0.5 M H_2SO_4 solution (purged in pure N_2 for 30 min before use) with the scan rate of 5 mV/s. The durability of the catalyst was assessed by cycling the electrode for 1000 times with each cycle started at +0.10 V and ended at −0.3 V with a scan rate of 50 mV/s. The electrochemical impedance spectrum (EIS) measurement was carried out at an overpotential of 150 mV with a frequency range from 10^5 Hz to 0.1 Hz at an AC voltage of 5 mV. The TOF and C_{dl} were measured according to the method reported by previous work [9,24]. All the potentials were calibrated to reversible hydrogen electrode (RHE) according to the previous report [27]. The potential transfer from SCE to RHE was obtained according to the following equation: E (RHE) = E (SCE) + 0.267 V. Current density referring to the geometric surface area of the GCE was used in the following discussion. All data were presented without iR compensation.

3. Results and discussion

3.1. Morphology of 3D MoS_2/rGO hydrogels

Fig. 1 displays the morphologies of different MoS_2/rGO hydrogels. The pristine MoS_2 nanosheets show seriously stacked layered structures with the lateral size of several micrometers (Fig. 1A), which leads to less exposed active sites and inferior activity [4]. When 1 ml GO is added in the reaction system, the lateral of the obtained MoS_2 sheets for the MoS_2/rGO_1 hydrogel reduces to about 100–200 nm (Fig. 1B), and MoS_2 nanosheets present interconnected ripples and curved edges. Further increase the volume of GO to 2 ml, the MoS_2 nanosheets crosslink with each other with dense corrugations and sharp folds (Fig. 1C). When 3 ml GO is added in the reaction system, a well-defined and porous 3D network structure of MoS_2/rGO_3 hydrogel (the inset in Fig. 1D) can be obtained due to the self-assembly of GO nanosheets during the hydrothermal reduction process [28]. The as-prepared MoS_2/rGO_3 has a wide pore distribution from submicrometers to nearly one micrometers. Such 3D framework network would be beneficial for shortening the electron diffusion channel due to the highly electroactive area [29], leading to superior HER performance. Moreover, the 3D network would compensate the volume change [29] during the long time test in acid media. However, the 3D network becomes less obvious when the GO volume is added to 4 ml (Fig. 1E). The random interconnection and stacking of MoS_2 nanosheets on the surface of rGO would decrease the amount of active sites, while the excess amount of GO might block the charge transfer from electrolyte to MoS_2, leading to inferior HER activity [15]. Moreover, the TEM image in Fig. 1(F) shows that the MoS_2

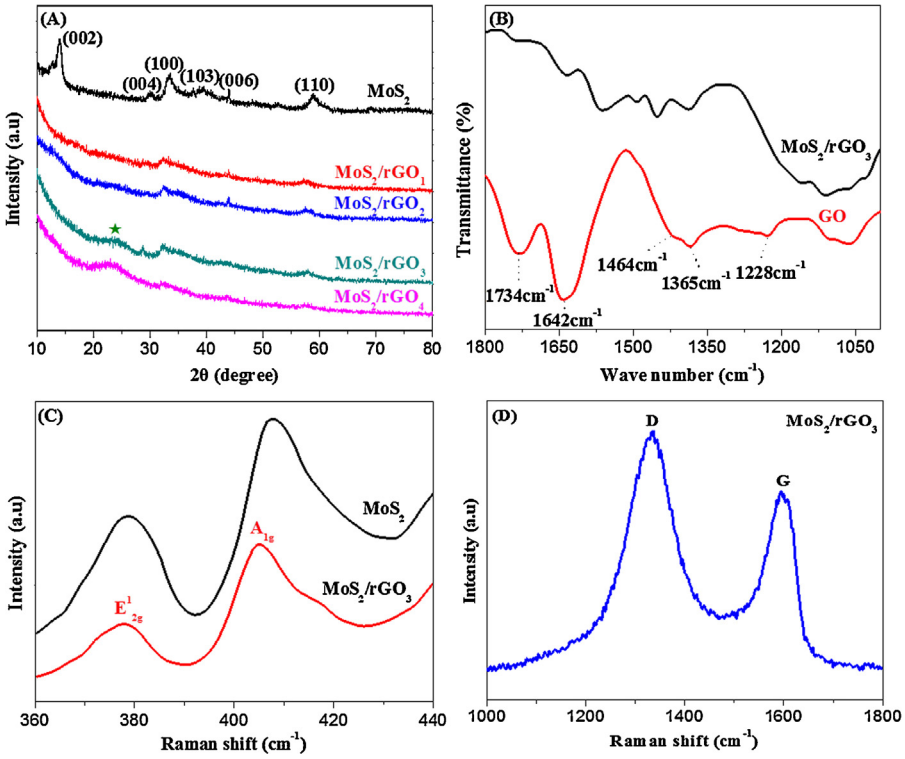

Fig. 2. (A) X-ray diffraction patterns of MoS_2 and various MoS_2/rGO composites, (B) Fourier transform infrared spectra of GO and MoS_2/rGO_3 hydrogels. (C)-(D) Raman spectra of MoS_2 and MoS_2/rGO_3 hydrogels.

nanosheets for MoS_2/rGO_3 are well anchored on the 3D rGO framework. The HRTEM image of MoS_2/rGO_3 hydrogel further confirms that MoS_2 nanosheets consist of few layers with an interlayer of 0.65 nm, which is in good agreement with the interlayer of (0 0 2) planes (Fig. 1G). Notice that the crystal fringes are discontinuous, indicating the existence of defects [13]. Such defects might provide more active sites, which makes MoS_2/rGO hydrogel appropriate as advanced catalysts for HER. The EDS result shows that the atom ratio of Mo/S is about 0.58 (Fig. 1H). The value is higher than the theoretical one (~0.5), which could be assigned to the trace amount of MoO_4^{2-} left in the 3D MoS_2/rGO_3 hydrogels or part of the MoS_2/rGO hydrogel oxidized in air [30]. This will be further confirmed by XPS in the following discussion.

XRD analysis was carried out to better understand the crystalline of the MoS_2/rGO hydrogel. As depicted in Fig. 2(A), pristine MoS_2 shows three characteristics peaks at $2\theta = 14.1°$, 33.6° and 59.0°, which can be assigned to the (0 0 2), (1 0 0) and (1 1 0) crystal planes of hexagonal MoS_2 (2H-MoS_2, JCPDS 37-1492), respectively. It is worth noting that the diffraction peak at $2\theta = 14.1°$ could be attributed to the stacked layers of (0 0 2) crystallographic plane along the C axis, suggesting the serious aggregation of pristine MoS_2 nanosheets during the hydrothermal process. However, MoS_2/rGO hydrogels show poor crystallinity and the (0 0 2) diffraction at $2\theta = 14.1°$ disappears, indicating the effect of rGO in inhibiting the growth of MoS_2 layers along the (0 0 2) planes [29]. Moreover, the diffraction peaks of (1 0 0) and (1 1 0) crystal planes of MoS_2/rGO hydrogels shift down to 32.7° and 57.6°, respectively. This may be the synergistic effect between MoS_2 nanosheets and rGO during hydrothermal process [21]. The FTIR spectrum of GO in Fig. 2(B) clearly shows three characteristic peaks at 1734 cm^{-1}, 1385 cm^{-1} and 1228 cm^{-1}, which can be assigned to —COOH (or —CO), C—OH and C—O (epoxide/ether) groups, respectively [31,32]. After hydrothermal reaction, such characteristic peaks disappear, indicating the successful reduction of GO to rGO. The Raman spectra in Fig. 2(C) obviously exhibit two characteristics peaks at 378 cm^{-1} and 405 cm^{-1} for MoS_2/rGO_3 hydrogel, corresponding to the in-plane E^1_{2g} and out-of-plane A_{1g} vibrations of 2H MoS_2, respectively [1,5]. However for pristine MoS_2, the corresponding characteristics peaks are at 378 cm^{-1} and 408 cm^{-1}, respectively. It is usually believed that the relatively broad peak E^1_{2g} and weaker intensity suggest the poor crystal structure [33]. Previous study reveals that the energy difference between two Raman peaks stands for the number of layers along the C axis [34]. The calculation values of energy difference between two Raman peaks for MoS_2/rGO_3 hydrogel and pristine MoS_2 are 27 cm^{-1} and 30 cm^{-1}, respectively, indicating that GO can effectively prevent MoS_2 nanosheets from restacking along C axis during the hydrothermal reaction, which is consistent with the results obtained from SEM and XRD analysis. Fig. 2(D) shows two typical Raman peaks for MoS_2/rGO_3 hydrogel at 1343 cm^{-1} (D band) and 1594 cm^{-1} (G band), respectively. The D band represents the defects, edges and disordered sp^2-hybridized carbon, while the G band can be assigned to the vibration of ordered sp^2-hybridized atoms [34]. The intensity ratio of I_D/I_G increases from 0.97 to 1.28, which may be attributed to the decreased size of GO [35] after the hydrothermal process, suggesting the successful reduction of GO to rGO.

The XPS spectra were further collected to illustrate the chemical states of as-prepared MoS_2/rGO_3. Fig. 3(A) shows two obvious peaks located at 228.3 eV (Mo $3d_{5/2}$) and 232.2 eV (Mo$3d_{3/2}$) [5]. However, another peak with weaker intensity can be observed at the higher binding energy of 235.6 eV. This may be attributed to the slow oxidation process from MoS_2 (IV) to MoO_3 (VI) or trace MoO_4^{2-} (VI) from unreacted precursor [30]. The S 2p spectrum in Fig. 3(B) shows two peaks at lower binding energies of 161.5 eV and 163.1 eV, which are assigned to S $2p_{3/2}$ and S $2p_{1/2}$ orbits, respectively [5]. Moreover, the peak at 164.3 eV suggests the existence of bridge or aspical S^{2-} due to the unsaturated sulfur atoms (S^{2-}) [5,36].

3.2. Electrochemical properties of MoS_2/rGO hydrogels

In order to reveal the morphology influence on the catalytic activity, electrochemical measurements were carried out. As is shown in Fig. 4(A), MoS_2/rGO_3 hydrogel has a small onset overpotential ($\eta = 125$ mV) compared to other four samples (Table 1), beyond which the cathodic current rises rapidly under more negative potentials, indicating the superior HER activity. The inset in Fig. 4(A) shows that the as-obtained MoS_2/rGO_3 hydrogel has a considerable current density about 45 A/g normalized by weight mass at 200 mV, which is nine times larger than the MoS_x grown on the graphene protected Ni foams [25]. Tafel plots are widespread used for quantitative kinetics analysis of the HER [37]. The Tafel slope for MoS_2/rGO_3 is estimated to be 41 mV/decade (Fig. 4B), which is much lower than other four samples. The Tafel slope represents the inherent character of the catalyst for HER [38,39]. Three possible principles are proposed for HER in acid media [1,5,37,38]:

$$H_3O^+ + e^- \rightarrow H_{ads} + H_2O \text{ (Volmer reaction)} \quad (1)$$

$$H_{ads} + H_3O^+ + e^- \rightarrow H_2 + H_2O \text{ (Heyrovsky reaction)} \quad (2)$$

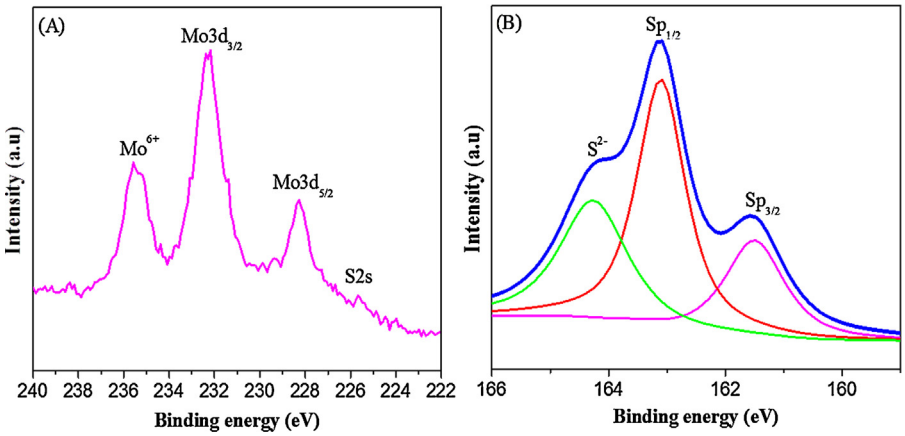

Fig. 3. X-ray photoelectron spectra of (A) Mo 3d and (B) S 2p, respectively.

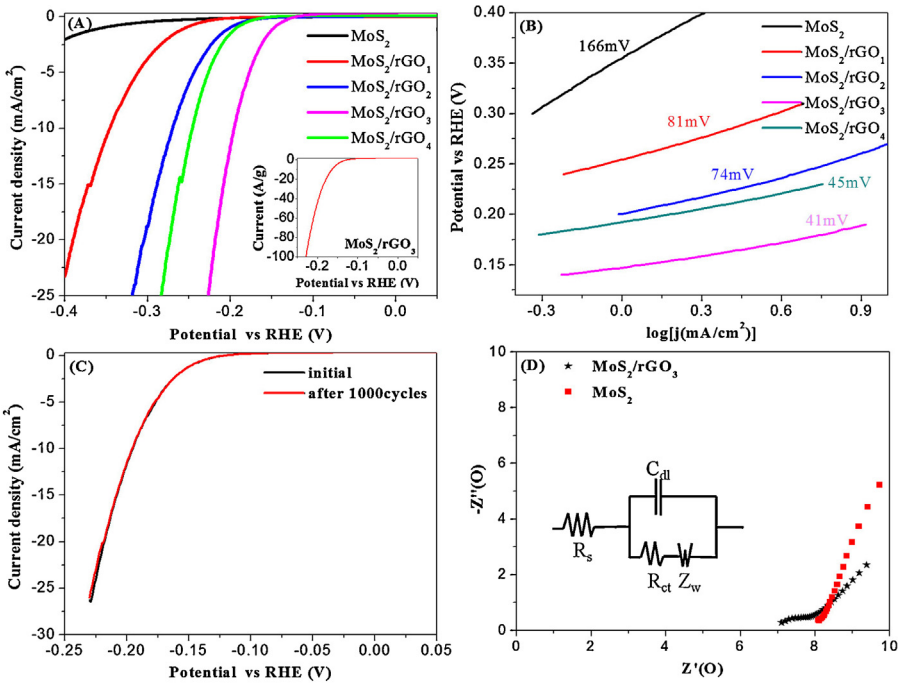

Fig. 4. (A) Polarization curves and (B) corresponding Tafel slopes of as-prepared MoS_2 and MoS_2/rGO composites in a 0.5 M H_2SO_4 solution, the inset in (A) is current density obtained from MoS_2/rGO_3 normalized by weight mass. (C) Stability test for MoS_2/rGO_3 hydrogel in a 0.5 M H_2SO_4 solution at a scan rate of 50 mV/s. (D) AC impendence spectra of as-prepared MoS_2 and MoS_2/rGO_3 composite in a 0.5 M H_2SO_4 solution with the frequency range from 10^5 HZ to 0.1 HZ and an amplitude of 5.0 mV (η = 150 mV). Inset is the equivalent model of system.

Table 1
Summary of valuable parameters of the as-prepared samples.

Catalyst[a]	η[b] (mV)	Tafel slope (mV/decade)	C_{dl}[c] (mF/cm^2)	C_{dl}[d] (mF/cm^2)	TOF[e] (S^{-1})	J[f] (mA/cm^2)
Pristine MoS_2	193	166	0.31	0.23	0.05	0.12
MoS_2/rGO_1	182	81	0.72	0.81	0.14	0.13
MoS_2/rGO_2	150	74	3.29	2.63	0.25	0.97
MoS_2/rGO_3	125	41	29.60	13.33	0.35	12.00
MoS_2/rGO_4	160	45	11.70	6.68	0.13	1.51

[a] All of the values were measured in a 0.5 M H_2SO_4 solution under the same conditions with the loading weight of 0.285 mg/cm^2.
[b] Onset potential was obtained at current density of 0.1 mA/cm^2.
[c] Double-layer capacitance (C_{dl}) was calculated from cyclic voltammetry experiments according to the precious paper [9].
[d] C_{dl} was calculated from electrochemical impedance measurements [30].
[e] Turnover frequency was recorded at η = 225 mV according to the previous report [24].
[f] Current density was recorded at η = 200 mV.

$$H_{ads} + H_{ads} \rightarrow H_2 \text{ (Tafel reaction)} \quad (3)$$

The value of Tafel slope for MoS_2/rGO is closed to 40 mV/decade (Fig. 4B), suggesting the Volmer-Heyrovsky HER mechanism during the HER process [1,37] and the electrochemical desorption step acted as rate-limiting step during the reaction [37,38]. Such small Tafel slope for MoS_2/rGO_3 hydrogel could be rationalized as follows: (1) intimate contact between MoS_2 nanosheets and rGO in the hydrogel not only enables perfect mechanical adhesion but also promotes electrical connection, facilitating the transfer of electrons from rGO substrate to MoS_2 nanosheets during cathodic polarization [29,37]; (2) limited layers along the (0 0 2) crystal planes and rich exposed active sites of MoS_2 act as catalytic centers which favor the process of hydrogen generation [3,6,29]; (3) the 3D configuration of MoS_2/rGO_3 hydrogel not only allows for easier diffusion of electrolyte into active center but also shortens the transfer path for electrons on the whole catalyst [22,25], leading to more efficient use of active centers. We further investigated the durability of MoS_2/rGO hydrogel. The as-synthesized MoS_2/rGO_3 catalysts show negligible loss even after continuous 1000 cycles and maintain the current density at 98.3% compared with its initial value (Fig. 4C), indicating the superior long-time stability of the MoS_2/rGO hydrogels in acid media. This could be attributed to the 3D network structures [21] and intimate contact [2,4] between the MoS_2 nanosheets and rGO hydrogel, decreasing the volume change during the long time test in acid media [29]. The electrode kinetics can be further demonstrated by EIS measurement. As shown in Fig. 4(D), the R_s (the series resistance of the system), which represents the ohmic resistance of electrolyte between the

Table 2
A brief summary of HER performance from various MoS_2 or MoS_2/rGO composites.

Catalyst	Catalyst loading (mg cm^{-2})	η (mV)	Tafel slope (mV/decade)	C_{dl} (μF/cm^2)	Reference
Li-MoS_2	3.400		62	29	[9]
Oxygen-incorporated MoS_2	0.285	120	55	534	[38]
Ultrathin MoS_2 perpendicular to graphene	0.204		43	6045	[41]
Defect-rich MoS_2 ultrathin nanosheets	0.285	120	50	N/A	[13]
E-MoS_2/GCE	0.048	120	70	N/A	[8]
MoS_2/rGO_3 hydrogel	0.285	125	41	29600	this work

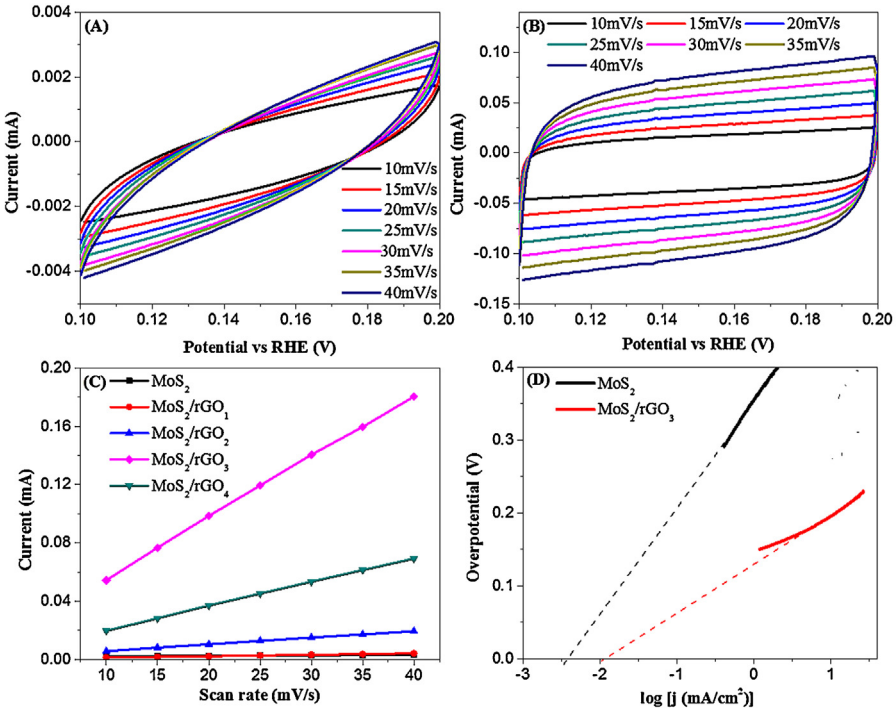

Fig. 5. Cyclic voltammograms of (A) pristine MoS_2 and (B) MoS_2/rGO_3 hydrogels in a 0.5 M H_2SO_4 solution at different scan rates. (C) Relations of difference between anodic and cathodic currents at 0.15 V with various scan rates from 5 mV/s to 40 mV/s. The slope is double C_{dl}. (D) Exchange current density for pristine MoS_2 and MoS_2/rGO_3 hydrogels obtained from the Tafel curves in Fig. 4B by using the extrapolation method.

electrode and Luggin capillary and that within the pores of the catalysts, are 8 Ω and 7 Ω for the systems related to pristine MoS_2 and MoS_2/rGO_3 hydrogel, respectively, manifesting excellent conductivity of electrolyte. Additionally, the semicircle for MoS_2/rGO_3 hydrogel is much smaller than that of pristine MoS_2, suggesting the rather low charge transfer resistance (R_{ct}) between the solid-liquid interface for MoS_2/rGO_3 electrode [30], which is in good agreement with the HER results shown in Fig. 4(A).

We further investigate the C_{dl} to explain the synergetic effect between MoS_2 and rGO nanosheets. There are two effective ways to get the C_{dl} in the HER process: by the calculation from EIS [30], or by the determination from cyclic voltammetry (CV) experiments. The difference usually exists when using these two methods due to different electrochemistry process (C_{dl} is obtained from EIS where HER takes place, while C_{dl} is determined from CV operated at Non-Faraday region). We obtain the C_{dl} of various MoS_2/rGO hybrids at the overpotential of 150 mV where HER takes place (Table 1). The MoS_2/rGO_3 shows the largest C_{dl}, indicating the enlarged electrochemically active surface area of the electrode compared with others due to the construction of 3D network structure. For better comparation with others' results, the C_{dl} obtained by CV experiments is shown in Table 1 and Table 2, which is estimated to be nearly proportional to effective active surface area [9,38,40,41]. As is depicted in Fig. 5(A) and Fig. 5(B), pristine MoS_2 presents a sharp cycle curves in the potential range from 0.1 V to 0.2 V, while the as-synthesized MoS_2/rGO_3 hydrogel exhibits a rectangle-like current-potential curves during the Non-Faraday process, indicating the larger C_{dl} than that of pristine MoS_2 nanosheets [9,40]. The C_{dl} for MoS_2/rGO is further obtained from the slopes of the curves related to difference between anodic and cathodic currents ($\Delta J = Ja - Jc$) at 0.15 V (*vs* RHE) and scan rate (Fig. 5C) [9]. The C_{dl} for MoS_2/rGO_3 is 29.60 mF/cm^2 (Table 2), which is about 129 times larger than that of pristine MoS_2 (Table 1) and much larger than the other counterparts due to the appropriate atom ratio of C:Mo and the formation of 3D matrix. Such extremely high C_{dl} indicates enlarged electrochemical area [24] and rich exposed active sites [38], which is further responsible for better HER performance. The C_{dl} obtained here is much larger than MoS_2 or MoS_2/graphene

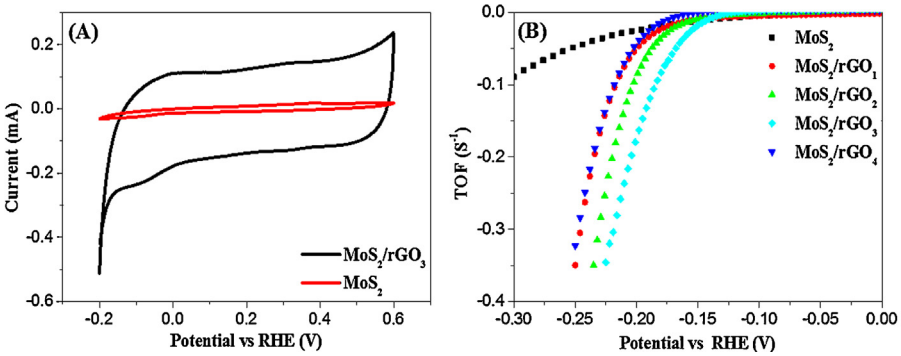

Fig. 6. (A) Cyclic voltammograms of MoS_2 and MoS_2/rGO_3 hydrogels in a 0.5 M H_2SO_4 solution at the scan rate of 50 mV/s. (B) Calculated turnover frequencies (TOF) of various hydrogels.

based HER catalysts reported in previous studies (Table 2). The exchange current density can be further calculated via the Tafel curves in Fig. 4B by the extrapolation method (Fig. 5D) [3,13]. The MoS_2/rGO_3 hydrogel displays larger current density of 12.04 μA/cm^2 compared with 3.96 μA/cm^2 for pristine MoS_2, indicating superior HER activity for MoS_2/rGO hydrogel once again [38].

Additionally, the synergetic effect between MoS_2 and rGO nanosheets was certified by rough estimation of TOF. TOF is usually calculated by quantifying the active sites (which are proportional to the integrated charge) through electrochemical approach [24]. The MoS_2/rGO_3 hydrogel shows a sharper cyclic voltammogram than that of pristine MoS_2 (Fig. 6A), indicating more active edge sites for MoS_2/rGO_3 hydrogel [5,24]. The MoS_2/rGO_3 hydrogel has a TOF of 0.35 S^{-1} at an overpotential of 225 mV (Fig. 6B), while amorphous MoS_2 films reaches the value of 0.3 S^{-1} at an overpotential of 340 mV [24]. However, the MoS_2/rGO_4 hydrogel exhibits a small TOF of 0.13 S^{-1} (Table 1), which is lower than those of MoS_2/rGO_1 and MoS_2/rGO_2 at the same overpotential. As was reported before, TOF represented intrinsic HER activity [5,39]. Though further increasing of GO concentration could continue to form the MoS_2/rGO_4 hydrogel, the C_{dl} and TOF for MoS_2/rGO_4 hydrogel decrease conversely. This could be attributed to excessive content of GO which not only hinders the exposure of active sites but also reduces the electrochemical active area (C_{dl} = 11.7 mF/cm^2) due to the stack of (0 0 2) planes of rGO after reduction during hydrothermal process. Thus, the concentration of GO in the reaction system plays a key factor in improving the HER activity and optimizing the performance of HER catalyst.

4. Conclusion

In summary, we have proposed a facile strategy to create the 3D network of MoS_2/rGO hydrogel with extremely high double-layer capacitance. The influences of the graphene oxide (GO) content on morphology, structure and HER performance of MoS_2/rGO hybrids have been carefully studied. The high turnover frequency and double-layer capacitance confirm the synergetic effect between MoS_2 nanosheets and rGO in the MoS_2/rGO hydrogel stemmed from its enlarged electrochemical area and rich active sites. Experimental data show that MoS_2/rGO_3 hydrogel with double-layer capacitance of 29.60 mF/cm^2 and TOF of 0.35 S^{-1} at an overpotential of 225 mV has an excellent HER activity with small onset overpotential of 125 mV, a large cathodic current density, especially, a small Tafel slope as low as 41 mV/decade. The superior HER activity could be ascribed to the appropriate content of GO that builds a 3D MoS_2/rGO hydrogel with more electrochemical area and additional exposed active sites. This work successfully demonstrates the content effect of GO in building 3D network structure as an advanced HER catalysts, and may open up a potential pathway for designing other transition metal sulfides/rGO hydrogels.

Acknowledgments

This work was supported by the National Natural Science Foundation of China (Nos. 51272237, 51572242 and 51175472), the 521 Talent Project of Zhejiang Sci-Tech University, the Scientific Research Foundation for the Returned Overseas Chinese Scholars (State Education Ministry) and the Program for Innovative Research Team of Zhejiang Sci-Tech university.

References

[1] Y.G. Li, H.L. Wang, L.M. Xie, Y.Y. Liang, G.S. Hong, H.J. Dai, Journal of American Chemical Society 133 (2011) 7296.
[2] Q.J. Xiang, J.G. Yu, M. Jaroniec, Journal of American Chemical Society 134 (2012) 6578.
[3] A.B. Laursen, S. Kegnaes, S. Dahl, I. Chorkendorff, Energy & Environmental Science 5 (2012) 5577.
[4] S.X. Min, G.X. Lu, The Journal of Physical Chemistry C 116 (2012) 25415.
[5] Y. Yan, B.Y. Xia, X.M. Ge, Z.L. Liu, J.Y. Wang, X. Wang, ACS Applied materials & interfaces 5 (2013) 12794.
[6] Z.Z. Wu, B.Z. Fang, Z.P. Wang, C.L. Wang, Z.H. Liu, F.F. Liu, W. Wang, ACS Catalysis 3 (2013) 2101.
[7] N. Liu, L.C. Yang, S.N. Wang, Z.W. Zhong, S.N. He, X.Y. Yang, Q.S. Gao, Y. Tang, Journal of Power Sources 275 (2015) 588.
[8] Z. Yang, C. Zhang, Z.Y. Liu, W.W. Tiju, I.Y. Phang, Z. Zhang, J.S. Pan, T.X. Liu, Electrochimica Acta 209 (2013) 269.
[9] H.T. Wang, Z.Y. Lu, D.S. Kong, J. Sun, T.M. Hymel, Y. Cui, ACS Nano 8 (2014) 4940.
[10] D.V. Esposito, J.G. Chen, Energy& Environmental Science 4 (2011) 3900.
[11] B. Hinnemann, P.G. Moses, J. Bonde, K.P. Jorgensen, J.H. Nielsen, S. Horch, I. Chorkendorff, J.K. Norskov, Journal of American Chemical Society 127 (2005) 5308.
[12] T.F. Jaramillo, K.P. Jorgensen, J. Bonde, J.H. Nielsen, S. Horch, I. Chorkendorff, Science 317 (2007) 100.
[13] J.X. Xie, H. Zhang, S. Li, R.X. Wang, X. Sun, M. Zhou, J.F. Zhou, X. Wen, D. Lou, Y. Xie, Advanced Materials 25 (2013) 5807.
[14] Y. Yan, B.Y. Xia, Z.C. Xu, X. Wang, ACS Catalysis 4 (2014) 1693.
[15] F.K. Meng, J.T. Li, S.K. Cushing, M.J. Zhi, N.Q. Wu, Journal of American Chemical Society 135 (2013) 10286.
[16] H.X. Chang, H.K. Wu, Energy & Environmental Science 6 (2013) 3483.
[17] B.G. Choi, M.H. Yang, W.H. Hong, J.W. Choi, Y.S. Huh, ACS Nano 6 (2012) 4020.
[18] Y.M. He, W.J. Chen, X.D. Li, Z.X. Zhang, J.C. Fu, C.H. Zhao, E.Q. Xie, ACS Nano 7 (2013) 174.
[19] R.H. Wang, C.H. Xu, J. Sun, L. Gao, H.L. Yao, ACS Applied materials &interfaces 6 (2014) 3427.
[20] C.C. Kuang, P.Y. Lin, Y.H. Xue, R.H. Akolkar, L.H. Dai, X. Yu, C.H. Liu, Journal of Power Sources 256 (2014) 329.
[21] W.J. Zhou, K. Zhou, D.M. Hou, X.J. Liu, G.Q. Li, Y.H. Sang, H. Liu, L.G. Li, S.W. Chen, ACS Applied materials &interfaces 6 (2014) 21534.
[22] Y. Hou, B. Zhang, Z.H. Wen, S.M. Cui, X.R. Guo, Z. He, J.H. Chen, Journal of Materials Chenistry A 2 (2014) 13795.
[23] Z.H. Pu, Q. Liu, A.M. Asiri, A.Y. Obaid, X.P. Sun, Journal of Power Sources 263 (2014) 181.
[24] D. Merki, S. Fierro, H. Vrubel, X.L. Hu, Chemical Science 2 (2011) 1262.
[25] Y.H. Chang, C.T. Lin, T.Y. Chen, C.L. Hsu, Y.H. Lee, W.J. Zhang, K.H. Wei, L.J. Li, Advanced Materials 25 (2013) 756.
[26] W.S. Hummers Jr, R.E. Offeman, Journal of American Chemical Society 80 (1958) 1339.
[27] V. Kiran, D. Mukherjee, R.N. Jenjeti, S. Sampath, Nanoscale 6 (2014) 12856.
[28] X. Huang, Z.Y. Zeng, H. Zhang, Chemical Society Review 42 (2013) 1934.
[29] K. Chang, W.X. Chen, ACS Nano 6 (2011) 4720.
[30] X.L. Zhang, J.B. Xu, K.Y. Yan, H. Wang, Z.L. Wang, S.H. Yang, Chemistry of Materials 26 (2014) 2344.
[31] Y.T. Liu, X.D. Zhu, Z.Q. Duan, X.M. Xie, Chemical Communication 49 (2013) 10305.
[32] G.C. Huang, T. Chen, W.X. Chen, Z. Wang, K. Chang, L. Ma, F.H. Huang, D.Y. Chen, J.Y. Lee, Small 9 (2013) 3693.
[33] Y. Yan, X.M. Ge, Z.L. Liu, J.Y. Wang, J.M. Lee, X. Wang, Nanoscale 5 (2013) 7768.
[34] K.K. Liu, W.J. Zhang, Y.H. Lee, Y.C. Lin, M.T. Chang, C.Y. Su, C.S. Chang, H. Li, Y.M. Shi, H. Zhang, C.S. Lai, L.J. Li, NANO Letters 12 (2012) 1538.
[35] S. Stankovich, D.A. Dikin, R.D. Piner, K.A. Kohlhaas, A. Kleinhammes, Y. Jia, Y. Wu, S.T. Nguyen, R.S. Ruoff, Carbon 45 (2007) 1558.
[36] J. Kibsgaard, T.F. Jaramillo, F. Besenbacher, Nature Chemistry 6 (2014) 248.
[37] J.Q. Tian, Q. Liu, A.M. Asiri, X.P. Sun, Journal of American Chemical Society 136 (2014) 7587.
[38] J.F. Xie, J.J. Zhang, S. Li, F.B. Grote, X.D. Zhang, H. Zhang, Y. Lei, B.C. Pan, Y. Xie, Journal of American Chemical Society 135 (2013) 17881.
[39] J.D. Benck, T.R. Hellstern, J. Kibsgaard, P. Chakthannont, T.F. Jaramillo, ACS Catalysis 4 (2014) 3957.
[40] M.A. Lukowski, A.S. Daniel, F. Meng, A. Forticaux, L.S. Li, S. Jin, Journal of American Chemical Society 135 (2013) 10274.
[41] Z.H. Deng, L. Li, W. Ding, K. Xiong, Z.D. Wei, Chemical Communications 51 (2015) 1893.